Osteoarthritis and Cartilage (2008) **16,** 689–697

doi:10.1016/j.joca.2007.09.015

Osteoarthritis and Cartilage

International Cartilage Repair Society

OARSI OSTEOARTHRITIS RESEARCH SOCIETY INTERNATIONAL

Anisotropy of collagen fibre alignment in bovine cartilage: comparison of polarised light microscopy and spatially resolved diffusion-tensor measurements[1]

S. K. de Visser B.Eng. (Med.)†‡, J. C. Bowden B.Sc.†‡, E. Wentrup-Byrne Ph.D.†‡, L. Rintoul Ph.D.†‡, T. Bostrom Ph.D.†‡, J. M. Pope D.Phil.†‡ and K. I. Momot Ph.D.†‡*

† *School of Physical and Chemical Sciences, Queensland University of Technology, GPO Box 2434, Brisbane, Qld 4001, Australia*

‡ *Institute of Health and Biomedical Innovation, Kelvin Grove, Qld 4059, Australia*

Summary

Objective: To compare collagen fibre alignment angles obtained from polarised light microscopy (PLM) and diffusion-tensor imaging (DTI) in bovine articular cartilage.

Methods: Five samples of bovine articular cartilage from five different animals were studied using magnetic resonance imaging and PLM techniques. T_2-weighted, diffusion-tensor (DT), and PLM images were acquired for each sample and average depth profiles of the PLM and DTI angles, as well as the banding patterns observed in T_2-weighted magnetic resonance (MR) images, were compared. Statistical properties of the distributions of the DTI and PLM angles were examined.

Results: The samples exhibited a range of alignment morphologies. In the samples with the "conventional" three-zone alignment pattern, a correlation between the PLM and DTI alignment zones and the banding in T_2-weighted MR images was observed. The shapes of the depth profiles of the PLM and DTI alignment angles were qualitatively similar for each sample. Three samples showed good quantitative correlation between the DT and PLM alignment angles. The correlation between the diffusion and PLM alignment angles was best in the regions of low degree of disorder of fibre alignment.

Conclusions: This study provides the first quantitative comparison of DTI of cartilage with the more established PLM techniques. The correlation between alignment angles derived from PLM and DTI data was evident across a wide range of alignment morphologies. The results support the use of DTI for the quantitative measurement of collagen fibre alignment. The microscopic-scale ($\sim$10 μm) dispersion of fibre alignment angles appears to be an important factor for understanding the extent of quantitative correlation between PLM and DTI results.

Key words: Collagen fibre orientation, Diffusion-tensor imaging, Polarised light microscopy, Anisotropy, Birefringence, Fibre alignment order.

Abbreviations: AS, articular surface of cartilage; $\mathbf{B}_0$, the vector of the static magnetic field; DTI, diffusion-tensor imaging; FA, fractional anisotropy; MR(I), Magnetic resonance (imaging); NMR, Nuclear magnetic resonance; PLM, polarised light microscopy; *R*, correlation coefficient of linear regression; ROI, region of interest; R_{PLM}, goodness-of-fit of the PLM polarisation angle; SEM, scanning electron microscopy; α, PLM polarisation angle (the angle between the fast optical axis and the normal to the articular surface of the sample); θ, the angle between the principal diffusion eigenvector and the normal to the articular surface of the sample; θ_{AS}, the angle between the static magnetic field $\mathbf{B}_0$ and the normal to the articular surface of the sample.

Introduction

Adult articular cartilage has a zonal architecture which is determined by the alignment of its collagen fibres. Three zones of alignment are usually distinguished[1]. The fibres are aligned parallel to the articular surface (AS) in the superficial zone (closest to the AS) and normal to the surface in the radial zone (closest to the bone), with a continuous and monotonic variation in average fibre orientation in the transitional zone between them. This architecture was proposed initially on the basis of polarised light microscopy (PLM) and scanning electron microscopy (SEM) measurements[1–4].

PLM is a transmission optical microscopy technique that measures the birefringence of the sample. The wavelength of the light is selected so as to exclude specific interactions (e.g., absorption maxima); therefore, the tissue can be considered a continuous but optically anisotropic medium. The orientation of collagen fibres is inferred on the basis of the directions of optical axes at the maximal birefringence (or optical retardance, which is linearly proportional to birefringence in a sample of uniform thickness). PLM was the first technique used to establish (albeit within the context of a model that was incorrect in detail) the curved architecture of collagen fibres in adult cartilage[5] and remains one of the most commonly used techniques for the investigation of cartilage microstructure.

Magnetic resonance (MR) techniques [Nuclear magnetic resonance (NMR) and magnetic resonance imaging (MRI)]

[1]This work was supported by a QUT Strategic Collaborative Research Program Grant.

*Address correspondence and reprint requests to: Dr Konstantin I. Momot, Ph.D., School of Physical and Chemical Sciences, Queensland University of Technology, GPO Box 2434, Brisbane, Qld 4001, Australia. Tel: 61-7-3138-1173; Fax: 61-7-3138-1521; E-mail: k.momot@qut.edu.au

Received 14 March 2007; revision accepted 18 September 2007.

have been widely applied in studies of cartilage since the 1990s and have been used both clinically[6] and *in vitro*[7–16]. The phenomenon of banding observed in spin-density and relaxation-weighted MR images[17–22] has been successfully used as a probe of the zonal structure of cartilage. Diffusion-tensor imaging (DTI) is an MRI technique that has recently found application in microimaging of cartilage[7–9,23]. DTI yields specific and precise information about local anisotropy on the length scale of tens of microns, and is exquisitely sensitive to the local morphological structure of the studied tissue[24–26]. Two recent studies of cartilage have demonstrated that spatially resolved maps of the direction of the principal diffusion eigenvector derived from DTI measurements are consistent with the known collagen fibre architecture[7,9]. DTI measurements have also been used to observe changes in collagen fibre orientation under mechanical compression[8].

Both PLM and DTI, therefore, indirectly measure the prevailing orientation of collagen fibres, although in different ways. While PLM remains the "gold standard" for measurement of fibre orientation, there is significant interest in adapting non-destructive techniques for the observation of microstructure and molecular integrity of cartilage[7,9,14–16]. DTI possesses many of the features required for this task, namely: non-invasiveness; the ability to provide sub-millimetre spatial resolution; and sensitivity to both the microscopic environment and local structure of the tissues studied. In addition, interpretation of the directional anisotropy of the diffusion-tensor (DT)[7–9] is relatively straightforward compared to quantitative interpretation of MR relaxation rates[27]. A comparison of DTI with the more established PLM techniques is important for evaluating the advantages and limitations of each technique; however, to date no quantitative comparative analysis of PLM and DTI results relating to cartilage has been available.

In this work, we compare *in vitro* PLM and DTI results obtained from five samples of bovine articular cartilage that exhibited a range of morphologies. In each measurement, a two-dimensional (2D) spatially resolved image of the cartilage sample was obtained. Spatial resolution in the depth dimension (the direction perpendicular to the AS) enabled the measurement of the depth profiles of the PLM polarisation angle and the direction of DTI principal diffusion eigenvector. Spatial resolution in the lateral dimension (along the AS) enabled statistical analysis of the angular distributions at a given depth. The resulting depth profiles of the PLM polarisation angle and the direction of the principal diffusion eigenvector were compared with each other and with the banding patterns observed in T_2-weighted MR images of each sample. The statistical properties of the distributions of the DTI and PLM angles, as well as the relationship between the standard deviations of these angles and the degree of correlation between PLM and DTI profiles, were also examined.

Methods

SAMPLE PREPARATION

Five samples of bovine cartilage (A–E), obtained from the femoral condyles of five different animals, were examined. Four samples (A, B, D, and E) were taken from the upper medial edge of the lateral femoral condyle, and one (sample C) from the middle of the medial femoral condyle. The age of the animals at slaughter was in the range 6 months–2 years. The typical thickness of the cartilage in the samples was 2 mm. The joints had been collected fresh from the *abattoir* on the morning of the first day of testing. Cartilage samples approximately 1 cm × 1 cm in size were sawn off the patellar grooves to include an underlying layer of subchondral bone, as seen in Fig. 1. The samples were placed in phosphate buffered saline (PBS) for 1 h to allow re-hydration. These samples were used for MR imaging without further modification and kept in PBS during the imaging. PBS (0.01 M phosphate buffer, 0.0027 M KCl, 0.137 M NaCl, pH 7.4 at 25°C) was prepared from PBS concentrate tablets (Sigma–Aldrich, USA). For PLM, cartilage samples were cryo-sectioned perpendicular to the AS. The sections were defrosted, hydrated, and placed on glass slides without any additional fixing. The position and orientation of the sections analysed were chosen to correspond to the imaging plane used in the respective DTI measurements. The thickness of the sections was 20 μm.

PLM

PLM was carried out on a Nikon Labophot-pol microscope fitted with a blue 1W light-emitting diode (LED) light source ($\lambda \sim 475$ nm, $\Delta\lambda_{fwhh} \sim 25$ nm, LumiLED, USA), using a 5× objective and 12 bit thermo-electrically cooled digital camera (Leica DFC480, Leica Microsystems GmbH, Wetzlar, Germany) with crossed polarising elements and calibration wave-plate. The samples were centred in the microscope with the normal to the AS of the cartilage directed along the *x*-axis of the camera, which corresponds to the *x*-axis of Fig. 2. Retardance images of the sections were taken, leaving the sample stationary and rotating the crossed polarising elements in 15° angular increments with the polariser moving from −45° to 45° (analyser from 45° to 135°). This ensured pixel alignment between different photographs of the same sample. With the polariser and analyser in the final positions, two final images of the sample were taken with the analyser offset 5° either side from the crossed position and with a wave-plate inserted with slow axis at 90° to the *x* direction. These two images are referred to as "negative-image", where the analyser is 5° clockwise towards the *x*-axis, and a "positive-image", where the analyser is 5° anti-clockwise past the 90° crossed position. To determine the direction of the optical axis of the sample, a squared sine ($\sin^2$) function with a baseline offset was fitted for each pixel to the intensity of the image as a function of the polariser angle. The phase of the fitted $\sin^2$ function was taken as the analyser offset at that pixel. The "negative" and "positive" images were used unambiguously to convert the analyser offset into the polarisation angle α (the direction of the fast optical axis of the sample) and to distinguish between α values ϕ and $\phi + 90°$. The digital resolution was $(2.73\ \mu m)^2$ in each image.

MRI

MRI measurements were performed using a Bruker Avance NMR spectrometer with a 7.0 T vertical-bore magnet. The system was equipped with a 1.1 T m^{-1} (110 G cm^{-1}) triple-axis gradient set and a Micro2.5 microimaging probe. The radiofrequency (RF) coil used in the imaging was a 15 mm birdcage ^{1}H resonator (Bruker, Germany). Further details of the imaging system can be found in the literature[7,8,24]. Cartilage specimens were immersed in physiological saline inside a 15 mm NMR tube and orientated at the required angle with respect to the static magnetic field $\mathbf{B}_0$ using previously manufactured Teflon plugs[7,8].

T_2-WEIGHTED IMAGING

T_2-weighted images of each sample were recorded at 25°C with the normal to the AS of the sample orientated at $\theta_{AS} = 0°$ with respect to the static magnetic field ($\mathbf{B}_0$). The imaging slice was 2 mm thick and orientated perpendicular to the AS. The images were recorded using a multi-echo spin-echo (SE) sequence with an echo spacing of 4.3 ms. Image matrix size was 128 × 128; effective sweep width, 70 kHz; repetition time, 2500 ms; field of view, 20 mm × 20 mm. Four transients per scan were acquired; the total imaging time was 21 min per sample.

DTI

DT images were recorded at 25°C using a single-echo diffusion-weighted spin-echo sequence. The imaging slice was 2 mm thick and orientated perpendicular to the AS. To maximise the T_2 values, the samples were orientated so that the normal to the AS formed an angle $\theta_{AS} \approx 55°$ with $\boldsymbol{B}_0$[7]. Image matrix size was 128 × 128, zero-filled to 256 × 256 prior to Fourier transform; effective sweep width, 120 kHz; repetition time, 2000 ms; echo time, 12.58 ms; field of view, 20 mm × 20 mm. The diffusion parameters were: δ, 2 ms; Δ, 8 ms; diffusion gradient, $g_0 = 0.7$ T m^{-1}. The DT was sampled using six independent gradient directions. The values of the elements of the tensor were obtained from a linearised Stejskal–Tanner diffusion–attenuation equation[28] using two gradient points for each direction: zero-gradient and g_0. The DT was reconstructed using Matlab code written in-house and based on previously published work[7,24]. Signal averaging was achieved by adding eight transients for each diffusion gradient direction used; the imaging time was 34 min per direction (approximately 4 h per sample).

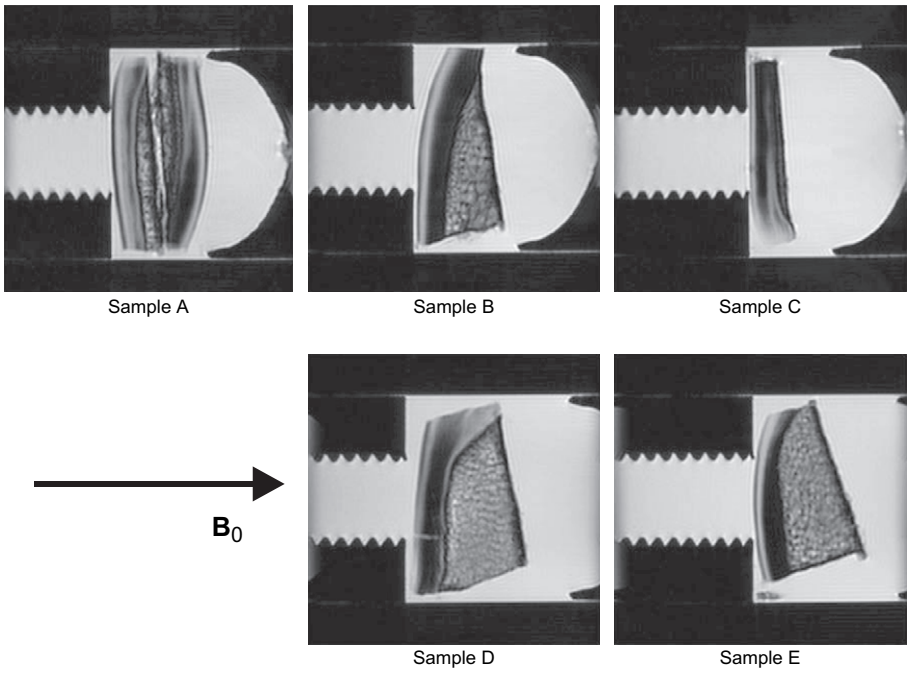

Fig. 1. T_2-weighted images of samples A–E. The images were acquired with the normal to the AS of the samples parallel to the static magnetic field $\mathbf{B}_0$ ($\theta_{AS} = 0^\circ$). The imaging slice was 2 mm thick and orientated perpendicular to the AS. The images were recorded using a multi-echo spin-echo sequence with spacing 4.3 ms. Imaging conditions: matrix size 128 × 128; effective sweep width, 70 kHz; repetition time, 2500 ms; field of view, 20 mm × 20 mm; four transients per scan. The images shown correspond to the 65th echo (echo time (TE) = 279.4 ms). The dark area above the AS is the Teflon plug used to orient the sample; the bright area around the sample is saline. Scale: the field of view shown is 2 cm in each dimension. Of the two samples in A, the left sample was used for subsequent DTI and PLM measurements.

Results and data analysis

The T_2-weighted images of each sample at $\theta_{AS} = 0^\circ$ are shown in Fig. 1. The five samples exhibited a range of banding behaviours. Two of the samples, B and E, exhibited a "conventional" three-band pattern with hypointense outside bands and a hyperintense band in the middle. Sample C exhibited a more complex, five-band behaviour with a hyperintense band near the AS and alternating hypo and hyperintense bands of comparable thickness closer to the bone. The cartilage of this sample had been removed from the bone. Sample D exhibited a similar pattern to C over most of the sample, but with a hypointense band near AS and a relatively thick middle hypointense band. Finally, sample A [the left specimen in Fig. 1(A)] exhibited a complex banding pattern with a large fraction of the sample's thickness covered by hyperintense bands.

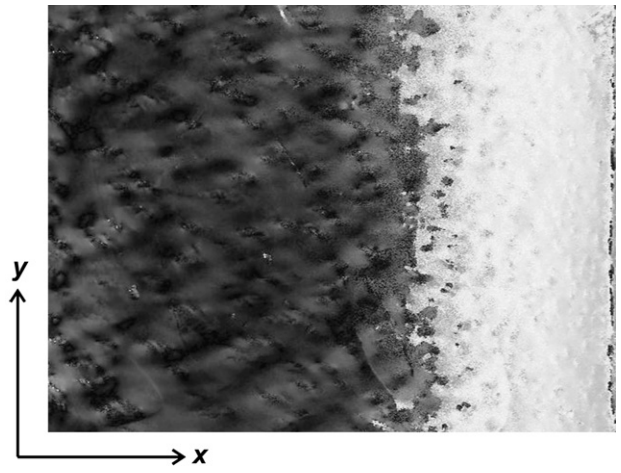

Fig. 2. Map of PLM polarisation angle α (the angle between the "fast" optical axis and the normal to AS) for sample B. White corresponds to $\alpha = 90^\circ$; black, to $\alpha = 0^\circ$.

DT images (78 μm in-plane spatial resolution after 2× zero-filling) and PLM images (2.7 μm spatial resolution) were obtained with the image plane perpendicular to the AS of the cartilage for each of the five samples studied. DTI images covered the full depth of the cartilage (from AS to the bone) and approximately 1.5 cm in the lateral dimension (the dimension along the AS). All PLM images covered an area 1.745 mm in the depth dimension × 1.309 mm in the lateral dimension.

From each DTI image, 2D spatially resolved maps of the following quantities were calculated: the angle between the principal eigenvector of the DT and the normal to the AS (diffusion angle, θ); fractional anisotropy (FA) of the DT(defined in Ref. 7); and the projection of the angle θ onto the imaging plane (θ_p). A representative map of the diffusion angle θ (sample B) is shown in Fig. 3. From each PLM image, spatially resolved 2D maps of the following quantities were calculated: the optical retardance (ρ); the polarisation angle between the "fast" optical axis and the normal to the AS (PLM angle, α); and the goodness-of-fit of the polarisation angle (R_{PLM}; defined for a given pixel as the standardised covariance, or Pearson's R value, between the sets of measured and fitted retardance values for the seven orientations of the polariser and analyser used in the measurements). An example of the polarisation angle map (sample B) is shown in Fig. 2.

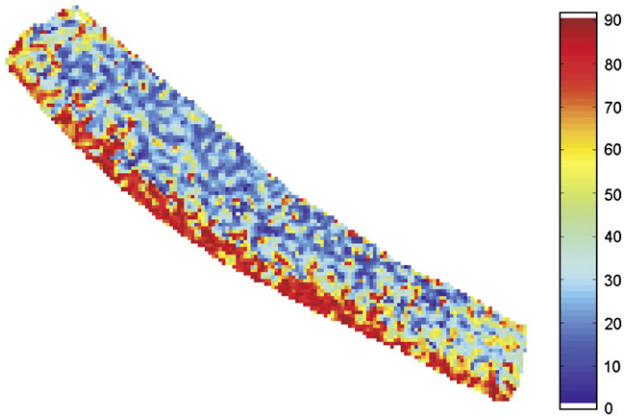

Fig. 3. Map of the diffusion angle θ (the angle between the principal diffusion eigenvector and the normal to AS) for sample B. The signal intensity scale is shown on the right, with white corresponding to $\theta = 0^\circ$ and black to $\theta = 90^\circ$. The signal from the surrounding water and bone has been removed by thresholding.

In addition to the spatially resolved 2D maps of PLM polarisation angle α and diffusion angle θ, one-dimensional (1D) depth profiles of the following DTI quantities were calculated: average diffusion angle $\langle\theta\rangle$ (and its standard deviation $\Delta\theta$); average fractional anisotropy $\langle$FA$\rangle$ (and ΔFA), as well as the average projected diffusion angle $\langle\theta_p\rangle$. The depth profiles of the sum of squared directional cosines of the diffusion eigenvectors ($\Sigma\cos^2$) (defined as the cosines of the angle between the normal to the AS and a given DT eigenvector) were also calculated. The regions of interest (ROIs) for the calculation of the average depth profiles were selected in the central regions of the samples, such that the ROIs were representative of the overall appearance of the image and free of any fissures or other abnormal features. The selected ROIs covered approximately 25 pixels (2 mm) in the lateral dimension of the sample. The average depth profiles of the following PLM quantities were also calculated: the angle α and its standard deviation ($\langle\alpha\rangle$ and $\Delta\alpha$), optical retardance ($\langle\rho\rangle$), and the goodness-of-fit ($\langle R_{\mathrm{PLM}}\rangle$). These depth profiles were calculated from the entire lateral width of the PLM field of view (1.309 mm).

The depth profiles of PLM polarisation angle $\langle\alpha\rangle$ and diffusion angle $\langle\theta\rangle$ are shown for each sample in Fig. 4. The PLM angle was averaged over 28 or 29 rows of PLM pixels, so that the calculated values of $\langle\alpha\rangle$ and $\langle\theta\rangle$ referred to similar cross-sectional areas of the respective sample. Both α and θ were also averaged in the lateral dimension as described in the previous paragraph. The depth profiles of $\langle\alpha\rangle$ and $\langle\theta\rangle$ fell into three groups. For samples B and E, both angles generally decreased with the increasing distance from the AS. For samples A and C, each of the angles α and θ had a minimum in the intermediate zone. The profiles for sample D were relatively featureless, with both the angles α and θ close to 90° through most of the thickness of the cartilage. In order to quantify the degree of agreement between the PLM and DT depth profiles, three types of statistical measures were used: (1) the parameters of the Bland–Altman plot[29]; (2) the number of data points for which the absolute value of the difference between the two angles, $|\theta - \alpha|$, was below 15°; and (3) kappa coefficients of agreement for categorically scaled data[30], where the data points were classified as belonging to one of three alignment zones: radial if θ, $\alpha < 30^\circ$; transitional if $30^\circ \leq \theta$, $\alpha \leq 60^\circ$; and superficial if θ, $\alpha > 60^\circ$. The values of these parameters for each sample are presented in Table I.

The depth profiles of FA of the DT ($\langle$FA$\rangle$), the goodness-of-fit parameter ($\langle R_{\mathrm{PLM}}\rangle$), the sum of the squared DTI directional cosines ($\Sigma\cos^2$), and optical birefringence ($\langle R\rangle$) were also calculated. The shape of these profiles generally was uncorrelated with the profiles of the angles $\langle\alpha\rangle$ and $\langle\theta\rangle$. The values of FA were typically in the range 0.05–0.14. The standard deviations, ΔFA, ranged from 15% to 40% of the value of FA at that depth, in a given sample. As a baseline, the nominal average value of the FA of a bulk-water region was also measured for each sample; the average baseline value was 0.07 ± 0.02. The sum of the squared DTI directional cosines, $\Sigma\cos^2$, exhibited a weak correlation ($R^2 = 0.37$) with the quantity $1 - \langle R_{\mathrm{PLM}}\rangle^2$.

Discussion

The PLM polarisation angle is a universally accepted measure of the alignment of collagen fibres in cartilage[5,31]. The orientation of the principal eigenvector in MR DT images was also recently shown to reflect the alignment of collagen fibres[7,9]. The objective of this study was quantitatively to compare the results obtained by the two techniques for a number of bovine cartilage samples, and to investigate the potential of DTI as a non-invasive, non-destructive imaging modality for quantitative measurement of collagen fibre orientation in articular cartilage. For a given sample, the comparison entailed acquiring PLM and DT images of ROIs of approximately the same location and orientation. This approach is consistent with the protocols used by other researchers, who found that the PLM images from parallel, 6-μm thick slices separated by up to 1 mm had the same general appearance[31].

DT imaging is based on the measurement of the random thermal motion of water molecules[32]. The motion is constrained by the immobile biopolymeric scaffold of the tissue. Molecular displacement (and therefore diffusive attenuation of the NMR spin-echo) is greatest in the direction in which the molecular motion is confined to the least extent. In cartilage, this anisotropic confinement of molecular motion results in the principal eigenvector of the DT generally assuming different orientations in each of the different zones of fibre alignment. The degree of the confinement can be measured by the FA of the DT. The FA values observed were small but significant and consistent with previous DTI studies of articular cartilage[7–9].

FIBRE ALIGNMENT MORPHOLOGY

The five samples of bovine cartilage showed a significant degree of variability in the behaviour of the depth profiles of the DTI and PLM alignment angles. The generally accepted model of collagen architecture in articular cartilage is that of collagen fibres perpendicular to the AS near the bone and gradually curving to become parallel to AS near the surface. This conventional model adequately described only two of the five samples studied (B and E). In sample A, the observed alignment patterns deviated from the conventional model near the bone. In samples C and D, the observed alignment patterns did not follow the conventional model at all.

This variation in the observed alignment patterns is consistent with previous studies of articular cartilage. Xia and co-workers reported an intrinsic spatial heterogeneity in the laminar appearance of cartilage in MR images, with

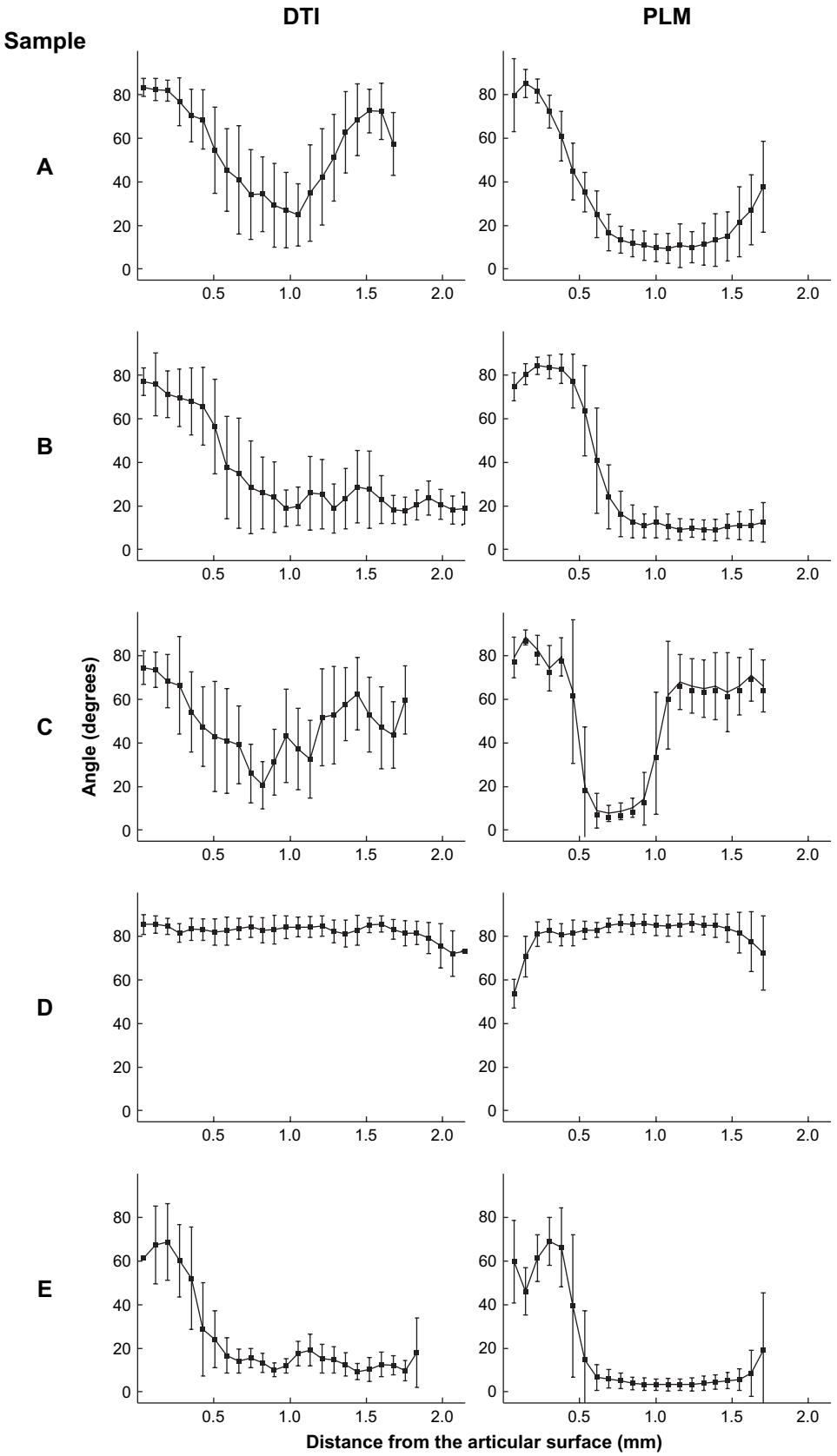

Fig. 4. Depth profiles of the average diffusion direction angle $\langle\theta\rangle$ (left column) and the average PLM polarisation angle $\langle\alpha\rangle$ (right column) for samples A–E (rows 1–5). Each plot consists of 22 equidistant individual points, which represent the average value of the respective angle in a given sample, at a given depth. The error bars represent the standard deviations, which were determined from the distributions of the angles over the respective laminae of the ROI.

Table I
Statistical agreement between the depth profiles of the PLM polarisation angle $\langle\alpha\rangle$ and diffusion angle $\langle\theta\rangle$ in each of the samples A–E. The number of points compared was 22 for each sample

Sample	Bland–Altman parameters (°)		$N_{agreement}$†	κ‡	Degree of agreement
	$\langle\theta-\alpha\rangle$	Limit of agreement*			
A	+23	32	5	0.18	General profile shape
B	+5	22	18	0.86	Good
C	−3	38	12	0.11	General profile shape
D	+2	16	21	0.93	Good
E	+6	18	20	0.73	Good

*Defined as twice the standard deviation of the Bland–Altman plot.
†The number of points (out of 22) for which $|\theta-\alpha|<15^\circ$.
‡Kappa coefficient of agreement for the data points classified as "radial", "transitional", or "superficial" (see Results and data analysis).

the number of laminae observed being dependent upon the location of the sample in the joint[20–22]. Foster *et al.* observed vertical striations on a sub-millimetre length scale[33]. Orientation of the split lines – i.e., the cleavage lines separating collagen leaves in the arch-like superstructure – also significantly affects the appearance of STM images of sectioned articular cartilage[1,19]. We shall refer to these factors collectively as "sample heterogeneity", i.e., a set of factors that may cause the observed fibre alignment profile to vary within a given sample of cartilage on the length scale of millimetres. Besides sample heterogeneity, the observed alignment morphologies may be influenced by the age, exact anatomical location of the sample, and individual anatomical and physiological peculiarities of the animals. An investigation of the factors influencing the observed morphologies is outside the scope of the present study. But importantly, it could not be assumed that collagen fibres always followed the same general orientational pattern. Consequently, the results of the PLM and DTI measurements need to be compared separately for each sample studied.

COMPARISON OF DTI AND PLM DEPTH PROFILES

Visual examination of Fig. 4 reveals that the shapes of the depth profiles of the PLM and DTI alignment angles were qualitatively similar for each of the five samples studied. In order to quantify the degree of agreement between the two sets of data, we employed the comparison parameters of Table I. Bland–Altman parameters and $N_{agreement}$ are based on the raw values of $\langle\alpha\rangle$ and $\langle\theta\rangle$; these parameters report on the quantitative degree of agreement between the two angles. The kappa coefficients are based on categorically scaled data and report on the agreement between the two techniques in identifying a particular layer of cartilage as belonging to radial, transitional, or superficial alignment zone. Table I shows that three of the samples (B, D, and E) exhibited a good quantitative correlation between the corresponding values of the DTI angle $\langle\theta\rangle$ and the PLM angle $\langle\alpha\rangle$. The other two samples (A and C) failed to show a significant agreement between the corresponding values of $\langle\theta\rangle$ and $\langle\alpha\rangle$. The presence of correlation between the overall shapes of the DTI and PLM profiles across a wide range of sample morphologies is encouraging, in that DTI was capable of reproducing the general alignment pattern in articular cartilage measured by another technique. The limits of agreement between DTI and PLM angles, as well as the lack of quantitative agreement in two of the samples studied, are discussed in the following sections of the paper.

COMPARISON WITH T_2-WEIGHTED IMAGES

It is useful to compare the DTI and PLM profiles shown in Fig. 4 with the banding observed in the T_2-weighted images of the same samples (shown in Fig. 1). The laminae seen in T_2-weighted images of cartilage have been shown to be statistically equivalent to the histological zones observed in the PLM images of unstained cartilage sections[31,34]. The two samples that exhibited the conventional PLM and DTI alignment patterns (samples B and E) also showed conventional banding in the T_2-weighted images acquired at $\theta_{AS}=0^\circ$. In sample A, the hyperintense bands approximately corresponded to the DTI regions in which the apparent fibre orientation was close to 55°, and the hypointense bands, to the regions with θ close to either 0° or 90°. In samples C and D there was no obvious correlation between the PLM and DTI profiles and the T_2-weighted banding patterns. The DTI profile of sample C was similar to that of sample A; however the T_2-weighted image of sample C exhibited an order of the bands different from sample A. Sample D showed little structure in the DTI and PLM profiles but a complex banding pattern in the T_2-weighted image. It therefore appears that the correlation between PLM alignment zones and T_2-weighted banding, which has been observed previously[31], may be present only in samples with the conventional alignment pattern but absent in "non-conventional" samples.

MICROSCOPIC DISORDER OF FIBRE ALIGNMENT

The error bars shown in Fig. 4 reflect the fact that, at a given depth within a particular sample, neither the PLM polarisation angle α nor the DTI diffusion angle θ were perfectly uniform. The standard deviations of each angle at a given depth typically fell within the range from 5° to 20°. We shall refer to this as "fibre alignment disorder", i.e., the presence of a distribution of fibre orientations at a given depth in a given sample. In some samples, this distribution may be contributed to by the presence of uniform but distinct domains within a given volume of cartilage (sample heterogeneity). However, the assumption of a multi-domain structure is not required, because on the microscopic-length scale collagen fibres are subject to a statistical distribution of orientations, even if the observed alignment pattern is uniform on the length scale of hundreds of microns or millimetres. For example, the paper by Xia *et al.* concluding that the prevailing collagen orientation does not vary significantly over a 1 mm distance, also clearly shows local non-uniformity of the PLM images on the length scale of tens of microns[31]. The SEM micrographs observed in numerous studies also reveal the presence of

a distribution of fibre orientations on the length scale 5–10 μm[1,35]. The presence of a microscopic-orientational distribution does not preclude the observed alignment pattern from being uniform in a given sample. The conservation of the prevailing fibre orientation over a macroscopic (1 mm) region requires only that the *average* orientation be conserved; it does not require a perfectly uniform alignment of all collagen fibres in that region.

In both the PLM and DTI profiles the relatively large values of the standard deviations of θ and α ($\Delta\theta$, $\Delta\alpha \geq 15^\circ$) tended to coincide with the regions where the alignment angles θ, α were between 30° and 60°. This suggests that the degree of disorder of fibre orientation is greatest in the transitional zones, where the fibres undergo a change in their alignment.

The presence of a microscopic disorder of fibre alignment is significant for the interpretation of DTI measurements. In a mesh of fibres disordered on a length scale of 10 μm, a particular water molecule will access a range of fibre orientations on the timescale of a DTI measurement. This will result in the measured DT and the DTI angle θ behaving as weighted-average quantities within a given DTI pixel, with the averaging depending in a complicated and non-linear way on the relative anisotropy and the degree of disorder. On the other hand, the apparent PLM angle is a simple vector average of the contributions from the individual fibres. Because of the different averaging behaviour of the PLM and DTI angles, the two techniques could yield identical values of the alignment angles only in the limit of perfectly uniform fibre alignment, but not when microscopic disorder is present. We therefore believe that disorder of fibre alignment on a microscopic (~10 μm) scale is important in order to understand the extent of agreement between the $\langle\alpha\rangle$ and $\langle\theta\rangle$ profiles of Fig. 4.

CORRELATION BETWEEN PLM AND DTI ANGLES

It is instructive to compare the full sets of angles $\langle\alpha\rangle$ and $\langle\theta\rangle$ for all five samples. A cumulative correlation plot between the average diffusion–orientation angle, $\langle\theta\rangle$, and the average PLM polarisation angle, $\langle\alpha\rangle$ is shown in Fig. 5(a). This plot includes all the individual data points shown in Fig. 4. Linear regression on the plotted points yielded $R^2 = 0.77$. Figure 5(a) also reveals a small but systematic positive difference between the DTI angle θ and the PLM angle α in the low-angle region of the plot.

Figure 5(b) shows the subset of the points of Fig. 5(a) for which the standard deviation $\Delta\theta$ was less than 15°. These points can be thought of as representing the laminae of cartilage where the fibre alignment was relatively uniform. Because the relatively large values of $\Delta\theta$ tended to occur in the transitional zones, the points of Fig. 5(b) contain mostly (albeit not exclusively) the points from the radial and superficial zones. Linear regression of the points of Fig. 5(b) yielded $R^2 = 0.90$. This suggests that the agreement between $\langle\alpha\rangle$ and $\langle\theta\rangle$ was best in the regions of low degree of disorder of fibre alignment. Conversely, in the transitional zones, where the disorder was relatively high, the agreement between $\langle\alpha\rangle$ and $\langle\theta\rangle$ was relatively poor. We hypothesise that one of the reasons for this is the different averaging behaviour of the angles $\langle\alpha\rangle$ and $\langle\theta\rangle$, which means that the difference between the two angles is greatest when the width of the statistical distribution of fibre orientations is large.

The PLM polarisation angle can be thought of as a projection of the three-dimensional (3D) direction of a collagen fibre onto the 2D plane as sampled in microscopy measurements. Conversely, DTI measurements yield the complete 3D orientation of the DT in each of the pixels in the imaging slice. Therefore, it can be argued that the proper way to compare PLM and DTI results is to use the diffusion angle θ projected onto the DT imaging plane. To test this hypothesis, the projected value θ_p of the angle θ was calculated for each DTI pixel, for each sample. The average depth profiles of θ_p were then calculated in the same way as for the original angle θ. The use of projected θ_p values did not improve, and in most samples worsened, the agreement between α and θ. This finding is consistent with the data of Fig. 5: If the angle α were indeed the PLM equivalent of the projected DTI angle θ_p, then the value of α would have significantly underestimated the true fibre orientation angle in the areas where the fibres run almost parallel to the AS

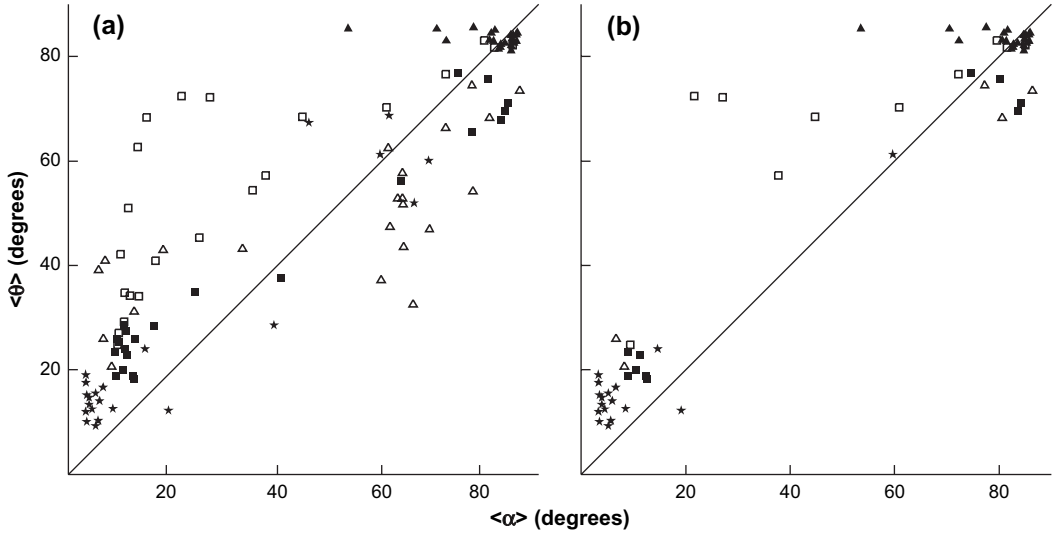

Fig. 5. (a) Average diffusion angle, $\langle\theta\rangle$, plotted vs average PLM polarisation angle, $\langle\alpha\rangle$, for all five samples: sample A, □; sample B, ■; sample C, △; sample D, ▲; sample E, ★. Each point refers to a given distance from the AS in a particular sample. The squared coefficient of linear regression $R^2 = 0.77$. The solid line corresponds to $\langle\theta\rangle = \langle\alpha\rangle$ and is given as a visual guide. The empty symbols correspond to the samples that failed to show a good agreement between the values of $\langle\theta\rangle$ and $\langle\alpha\rangle$ (samples A and C). (b) The same plot, but with all points with $\Delta\theta > 15^\circ$ excluded. The squared coefficient of linear regression $R^2 = 0.90$.

($\alpha = 90^\circ$). The subset of such fibres that are also almost perpendicular to the imaging plane would have appeared to be almost perpendicular to the AS as well (apparent $\alpha = 0^\circ$). But in fact, the agreement between $\langle\alpha\rangle$ and $\langle\theta\rangle$ near $\alpha = 90^\circ$ was good, meaning that no such underestimation occurred.

PRACTICAL CONSIDERATIONS IN DTI OF CARTILAGE

Diffusion measurements have long been a valuable tool in *in vitro* studies of cartilage[36,37]. Recent developments in diffusion NMR also open the possibility of selective measurement of diffusion of metabolites in cartilage from ^{1}H NMR spectra[38,39]. The present study was focused on the use of diffusion MR for studying the microstructure of cartilage samples *in vitro* and examined the agreement between the alignment angles derived from DTI and PLM measurements. The results demonstrate that DTI is capable of providing spatially resolved information characterising the alignment of collagen fibres, reinforcing the findings of other recent DTI studies[7–9,23]. As an *in vitro* study, the present work did not aim to optimise the imaging speed. We note, however, that the imaging times involved could be shortened significantly by combining the DTI protocol with fast (multi-slice SE) or ultrafast echo-planar imaging (EPI) acquisition techniques. This would be advantageous for increasing the achievable throughput in future similar studies. When extending the DTI methodology to cartilage samples on the bone, consideration will need to be given to the orientational dependence of the aqueous T_2 in cartilage. Maximising the T_2 by orienting the sample at the magic angle with respect to $\mathbf{B}_0$, as was done in the present study, may not always possible for irregular-shaped on-the-bone samples; this may limit the available signal-to-noise ratio. Consideration also needs to be given to the filling factor of the receiver; a small surface-coil detector would likely be the most appropriate for this type of sample.

Conclusions

The five samples of bovine articular cartilage exhibited a range of fibre alignment morphologies, with only two of the five samples studied showing the ''conventional'' three-zone pattern of PLM and DTI alignment angles. This study focused exclusively on examining the correlations between the results obtained from PLM and MR images, and did not examine the origins of the alignment variability. In the two ''conventional'' samples, the alignment zones derived from the average diffusion and PLM depth profiles were well-correlated with the banding observed in T_2-weighted MR images. No such correlation was readily apparent in the three samples with ''non-conventional'' depth profiles of the alignment angles. Three of the samples showed good quantitative agreement between the diffusion angle θ and the PLM angle α, and in all samples similarity of the shapes of the corresponding DTI and PLM alignment profiles was observed. The microscopic-scale ($\sim 10\ \mu$m) dispersion of θ and α and their respective averaging behaviour appears to be important factors for understanding the extent of quantitative agreement between the two alignment angles. The future development of an appropriate DTI data analysis methodology will benefit from the better understanding of the statistical averaging behaviour of the apparent DT realised in the current study. The findings are encouraging for the prospect of using DTI for the quantitative measurement of collagen fibre alignment.

Acknowledgements

We thank Dr Roger Meder for help with the setup of DTI experiments, Mr Don Geyer for help with the cryo-sectioning, Drs Diana Battistutta and Cameron Hurst for help with statistical treatment of the data, and Dr Mark Wellard for expert MR Facility management.

References

1. Jeffery AK, Blunn GW, Archer CW, Bentley G. Three-dimensional collagen architecture in bovine articular cartilage. J Bone Joint Surg Br 1991;73-B:795–801.
2. Freeman MAR, Ed. Adult Articular Cartilage. England: Pitman Medical Publishing; 1979.
3. Crouch JE. Functional Human Anatomy. 4th edn. Philadelphia: Lea & Febiger; 1985.
4. Clark JM. Variation of collagen fiber alignment in a joint surface – a scanning electron-microscope study of the tibial plateau in dog, rabbit, and man. J Orthop Res 1991;9:246–57.
5. Benninghoff A. Form und Bau der Gelenkknorpel in ihren Beziehungen zur Funktion. II. Der Aufbau des Gelenk-Knorpels in semen Beziehungen zur Funktion. Z Zellforsch Microsk Anat 1925;2:783–862.
6. Hall LD. Magnetic resonance imaging as a noninvasive means for quantitating the dimensions of articular cartilage in the human knee. Arthritis Rheum 2004;50:5–9.
7. Meder R, de Visser SK, Bowden JC, Bostrom T, Pope JM. Diffusion tensor imaging of articular cartilage as a measure of tissue microstructure. Osteoarthritis Cartilage 2006;14:875–81.
8. de Visser SK, Crawford RW, Pope JM. Structural adaptations in compressed articular cartilage measured by diffusion tensor imaging. Osteoarthritis Cartilage 2008;16:83–9.
9. Filidoro L, Dietrich O, Weber J, Rauch E, Oerther T, Wick M, *et al*. High-resolution diffusion tensor imaging of human patellar cartilage: feasibility and preliminary findings. Magn Reson Med 2005;53:993–8.
10. Nieminen MT, Toyras J, Laasanen MS, Silvennoinen J, Helminen HJ, Jurvelin JS. Prediction of biomechanical properties of articular cartilage with quantitative magnetic resonance imaging. J Biomech 2004;37:321–8.
11. Mlynarik V, Szomolanyi P, Toffanin R, Vittur F, Trattnig S. Transverse relaxation mechanisms in articular cartilage. J Magn Reson 2004; 169:300–7.
12. Xia Y, Moody JB, Alhadlaq H. Orientational dependence of T_2 relaxation in articular cartilage: a microscopic MRI (μMRI) study. Magn Reson Med 2002;48:460–9.
13. Nieminen MT, Toyras J, Rieppo J, Hakumaki JM, Silvennoinen J, Helminen HJ, *et al*. Quantitative MR microscopy of enzymatically degraded articular cartilage. Magn Reson Med 2000;43:676–81.
14. Shinar H, Seo Y, Ikoma K, Kusaka Y, Eliav U, Navon G. Mapping the fiber orientation in articular cartilage at rest and under pressure studied by H-2 double quantum filtered MRI. Magn Reson Med 2002;48: 322–30.
15. Navon G, Shinar H, Eliav U, Seo Y. Multiquantum filters and order in tissues. NMR Biomed 2001;14:112–32.
16. Ling W, Jerschow A. Selecting ordered environments in NMR of spin 3/2 nuclei *via* frequency-sweep pulses. J Magn Reson 2005;176:234–8.
17. Mlynarik V, Degrassi A, Toffanin R, Vittur F, Cova M, Pozzi-Mucelli RS. Investigation of laminar appearance of articular cartilage by means of magnetic resonance microscopy. Magn Reson Imaging 1996;14: 435–42.
18. Xia Y, Farquhar T, Burton-Wurster N, Lust G. Origin of cartilage laminae in MRI. J Magn Reson Imaging 1997;7:887–94.
19. Rubenstein JD, Kim JK, Moravaprotzner I, Stanchev PL, Henkelman RM. Effects of collagen orientation on MR-imaging characteristics of bovine articular-cartilage. Radiology 1993;188:219–26.
20. Xia Y. Heterogeneity of cartilage laminae in MR imaging. J Magn Reson Imaging 2000;11:686–93.
21. Xia Y. Magic-angle effect in magnetic resonance imaging of articular cartilage – a review. Invest Radiol 2000;35:602–21.
22. Xia Y, Moody JB, Alhadlaq H, Burton-Wurster N, Lust G. Characteristics of topographical heterogeneity of articular cartilage over the joint surface of a humeral head. Osteoarthritis Cartilage 2002;10:370–80.
23. Abdullah OM, Othman SF, Zhou XJ, Magin RL. Diffusion tensor imaging as an early marker for osteoarthritis. Proc Intl Soc Magn Reson Med 2007;15:814.
24. Moffat BA, Pope JM. Anisotropic water transport in the human eye lens studied by diffusion tensor NMR micro-imaging. Exp Eye Res 2002; 74:677–87.
25. Hagmann P, Thiran JP, Jonasson L, Vandergheynst P, Clarke S, Maeder P, *et al*. DTI mapping of human brain connectivity: statistical fibre tracking and virtual dissection. Neuroimage 2003;19:545–54.

26. Johansen-Berg H, Behrens TEJ. Just pretty pictures? What diffusion tractography can add in clinical neuroscience. Curr Opin Neurol 2006;19:379–85.
27. Burstein D, Gray ML. Is MRI fulfilling its promise for molecular imaging of cartilage in arthritis? Osteoarthritis Cartilage 2006;14: 1087–90.
28. Stejskal EO, Tanner JE. Spin diffusion measurements: spin echoes in the presence of a time-dependent field gradient. J Chem Phys 1965;42:288–92.
29. Bland JM, Altman DG. Statistical methods for assessing agreement between two methods of clinical measurement. Lancet 1986;1: 307–10.
30. Cohen J. A coefficient of agreement for nominal scales. Educ Psychol Meas 1960;20:37–46.
31. Xia Y, Moody JB, Burton-Wurster N, Lust G. Quantitative *in situ* correlation between microscopic MRI and polarized light microscopy studies of articular cartilage. Osteoarthritis Cartilage 2001;9:393–406.
32. Basser PJ, Mattiello J, LeBihan D. Estimation of the effective self-diffusion tensor from the NMR spin-echo. J Magn Reson B 1994;103: 247–54.
33. Foster JE, Maciewicz RA, Taberner J, Dieppe PA, Freemont AJ, Keen MC, *et al*. Structural periodicity in human articular cartilage: comparison between magnetic resonance imaging and histological findings. Osteoarthritis Cartilage 1999;7:480–5.
34. Grunder W. Mill assessment of cartilage ultrastructure. NMR Biomed 2006;19:855–76.
35. Kaab MJ, Gwynn IA, Notzli HP. Collagen fibre arrangement in the tibial plateau articular cartilage of man and other mammalian species. J Anat 1998;193:23–34.
36. Burstein D, Gray ML, Hartman AL, Gipe R, Foy BD. Diffusion of small solutes in cartilage as measured by nuclear-magnetic-resonance (NMR) spectroscopy and imaging. J Orthop Res 1993;11:465–78.
37. Xia Y, Farquhar T, Burtonwurster N, Verniersinger M, Lust G, Jelinski LW. Self-diffusion monitors degraded cartilage. Arch Biochem Biophys 1995;323:323–8.
38. Momot KI, Kuchel PW. PFG NMR diffusion experiments for complex systems. Concepts Magn Reson 2006;28A:249–69.
39. Momot KI, Kuchel PW. Convection-compensating PGSE experiment incorporating excitation-sculpting water suppression (CONVEX). J Magn Reson 2004;169:92–101.